Geophysical Journal International

Geophys. J. Int. (2017) **210,** 911–918
Advance Access publication 2017 May 16
GJI Seismology

doi: 10.1093/gji/ggx210

Surface temperature and precipitation affecting GPS signals before the 2009 L'Aquila earthquake (Central Italy)

A. Amoruso,[1] L. Crescentini[2] and L. Chiaraluce[3]

[1] *Dipartimento di Chimica e Biologia, Università di Salerno, I*-84084 *Fisciano, Italy. E-mail: aamoruso@unisa.it*
[2] *Dipartimento di Fisica, Università di Salerno, I*-84084 *Fisciano, Italy*
[3] *Istituto Nazionale di Geofisica e Vulcanologia, I*-00143 *Roma, Italy*

Accepted 2017 May 15. Received 2017 May 12; in original form 2017 February 14

SUMMARY

An M_w 6.1 normal faulting earthquake struck Central Italy in 2009 April, which unfortunately nucleated right below the town of L'Aquila, causing more than 300 casualties and widespread damage. The main shock was preceded by a foreshock sequence lasting ∼6 months. It has been claimed that an analysis of continuous Global Positioning System (GPS) data shows that during the foreshock sequence a 5.9 M_w slow slip event (SSE) occurred along a decollement located beneath the reactivated normal fault system. This hypothesized SSE that started in the middle of 2009 February and lasted for almost two weeks would have eventually loaded the largest foreshock and the main shock. We show that the strain signal that the SSE would have generated at two laser strainmeters operating at about 20 km NE from the SSE source was essentially undetected. We then propose an alternative interpretation for the displacement observed in the GPS data. A transient signal is present in temperature and precipitation time-series recorded close to the GPS station that has largest signal referred to the SSE, implying that these contaminated the GPS record. This work illustrates how environmental noise may be relevant when investigating small strain signals, showing the importance of having data from weather stations and water level sensors colocated with GPS stations.

Key words: Creep and deformation; Geodetic instrumentation; Transient deformation.

1 INTRODUCTION

It has been known for decades that faults may slip both seismically and aseismically. More recently, a varied set of deforming phenomena such as slow slip and silent events have been observed. These events, detected by seismic and geodetic stations, occur in different tectonic settings: along subduction zones (e.g. Ito *et al.* 2007; Schwartz & Rokosky 2007), transcurrent margins (e.g. Linde *et al.* 1996), oceanic transform faults (Shearer1994) and extensional systems (e.g. Crescentini *et al.* 1999).

It has also been observed that the same fault structure can undergo both seismic and aseismic slip, along different portions pertaining to the same system (e.g. Nadeau & Dolenc 2005). Slow slip events (SSE) have also been observed both before (Ito *et al.* 2013; Ruiz *et al.* 2014) and after large megathrust earthquakes (Hsu *et al.* 2006). Accordingly, the preparatory phase of a large earthquake may include both seismic (foreshocks) and aseismic (SSE) deforming episodes but, unlike afterslip (e.g. Amoruso & Crescentini 2009a), no slow event has yet been recorded before moderate earthquakes, even when they occurred close to high-sensitivity strainmeters (Johnston 1993; Johnston *et al.* 2006; Amoruso & Crescentini 2010; Agnew & Wyatt 2016).

An exception to this seems to be represented by the 2009 L'Aquila extensional earthquake (whose seismicity distribution is reported in Fig. 1) for which Borghi *et al.* (2016), after analysing continuous Global Positioning System (GPS) data from nearby stations by means of a principal component (PC) analysis, claimed that the April 6 M_w 6.1 (Scognamiglio *et al.* 2010) main shock was preceded, a couple of months before, by a 5.9 M_w SSE lasting for almost two weeks.

The 2009 L'Aquila earthquake that activated a 50 km long normal fault system was preceded by a foreshock sequence lasting for at least 6 months and culminating with an M_w 4.0 event, which occurred on March 30, a week before the main shock (Chiaraluce *et al.* 2011). Some authors proposed for the foreshocks that mostly occurred at the base of main normal fault plane activated by the main shock an active role in the nucleation process in terms of fluids involvement. Di Luccio *et al.* (2010) and Lucente *et al.* (2010), by analysing a few months of foreshock patterns in terms of temporal variations in seismic velocity and anisotropy, interpreted the changes as the signature of a complex sequence of dilatancy and fluid diffusion processes affecting the rock volume surrounding the nucleation patch. Also, Amoruso & Crescentini (2010) suggested a possible strain signature from a diffusive process in the last 3–4 d before the main earthquake. While Sugan *et al.* (2014) through the increasing of the seismic detection capability performed by applying a matched filter technique, observed from the middle of February, roughly the same period of time proposed by

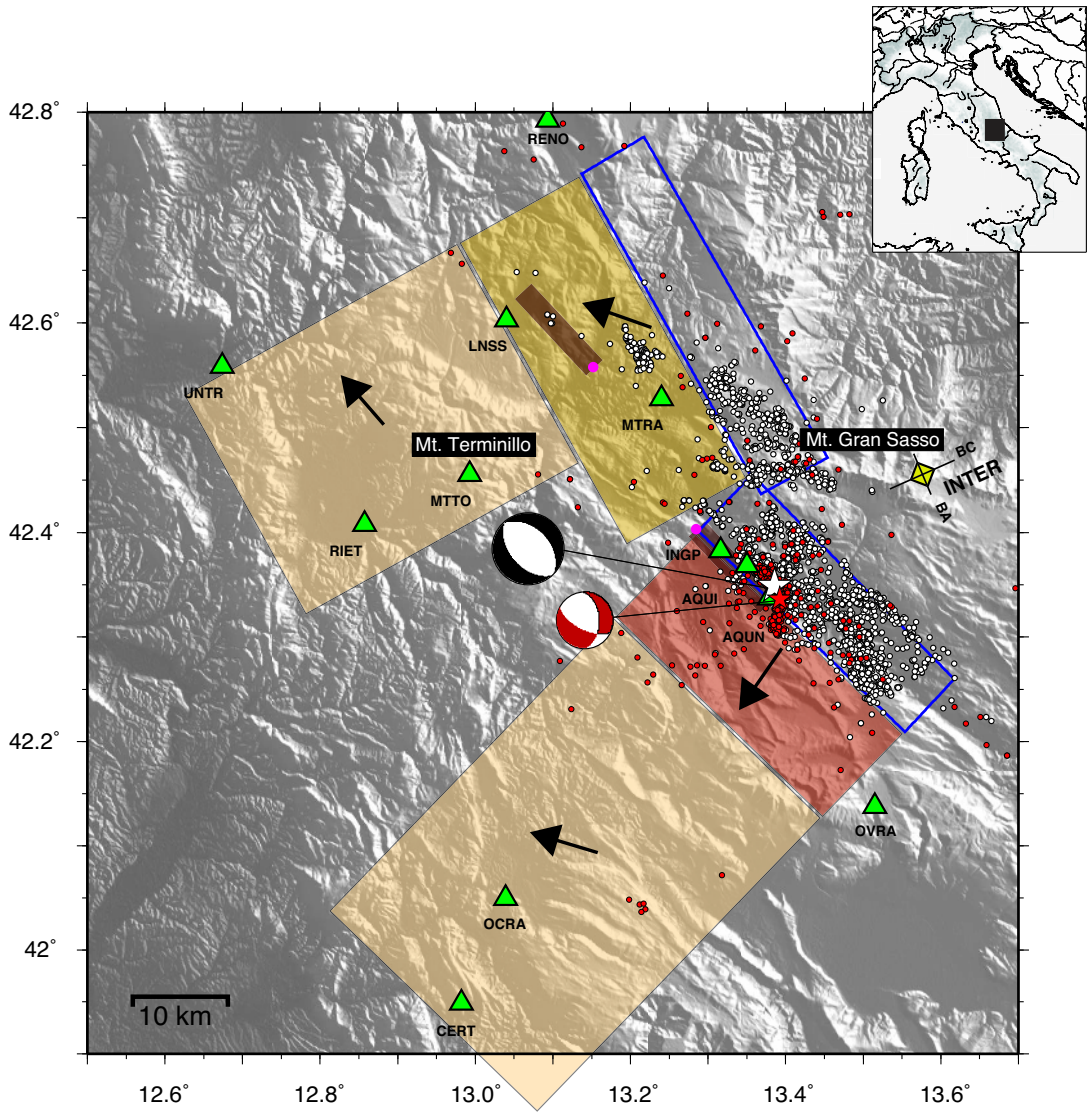

Figure 1. Map view of the study region containing the 2009 L'Aquila foreshocks (red circles) and aftershocks (white circles) sequence (from Chiaraluce *et al.* 2011) and the SSE source model (colour filled rectangles) and slip distribution (black arrows), proposed by Borghi *et al.* 2016 (courtesy of the authors). The two beach balls are the focal mechanisms of the M_w 4.0 and 6.1 foreshock and main shock of the sequence linked to their epicentre (red and white star, respectively). The GPS stations (green triangles) and the site of the interferometers (yellow diamond) are also shown. The two (black) lines named BA and BC centred on the interferometer location represent the orthogonal orientation of the two instruments.

Borghi *et al.* (2016) for the beginning of the SSE, a variation in the seismicity migration velocity (at about 0.5 km d^{-1}) toward the main shock hypocentre.

The motivation for this paper comes from the analysis by Amoruso & Crescentini (2010) of the strain data recorded by two high-precision laser interferometers (strainmeters), named BA and BC, that were operating beneath the Gran Sasso massif, close to the *Laboratorio Nazionale del Gran Sasso* of the *Istituto Nazionale di Fisica Nucleare*, at 1400 m depth and about 20 km to the NE of the epicentre (see instruments location in Fig. 1). These authors showed that the time-series recorded by these two instruments, did not show any anomalous signal on timescales of weeks, as showed in Fig. 2(b), where we show the recordings of BC that by reason of its orientation respect to the SSE source geometry, is supposed to be the better-oriented strainmeter.

Transient signals often recur in strain time-series, and sometimes they are related to environmental noise generated by temperature variations, precipitation (rain or snow), barometric pressure and soil moisture. These environmental disturbances may affect the instruments as well as the properties of the hosting lithologies for both surface (e.g. Agnew 1986; Ji & Herring 2012; Devoti *et al.* 2015) and underground installations (e.g. Dal Moro & Zadro 1998; Amoruso *et al.* 2014; Diaz *et al.* 2014). Moreover, seasonal variations observed in GPS time-series are often delayed with respect to temperature and may be largely attributable to thermoelastic strain in the ground (e.g. Prawirodirdjo *et al.* 2006), while monument thermal expansion could cause shorter period signals (e.g. Hill *et al.* 2009). Seasonal variations may also be controlled by groundwater recharge/discharge of karst aquifers as observed, for example, by new GPS observations for an area immediately south of the region where L'Aquila earthquake occurred, with potentially significant implications for the accurate estimation of tectonic deformation. Silverii *et al.* (2016) by means of new GPS observations showed multiyear deformation of non-tectonic but hydrological origin

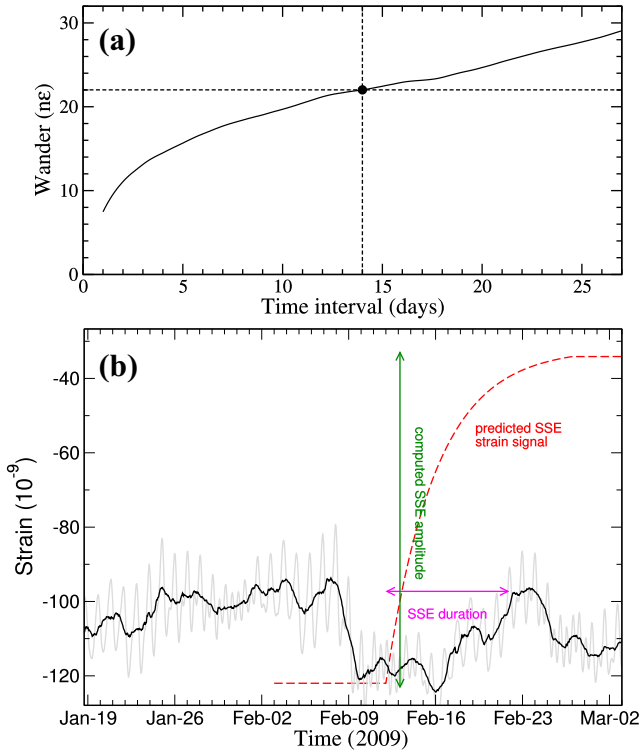

Figure 2. Comparison between the predicted SSE strain signal and data. (a) Wander in strain for different time intervals based on BC data collected between 2008 October 21 and 2009 April 5, low-pass filtered, and downsampled to 1800 s sampling. (b) Strain data recorded by the BC interferometer located below the Gran Sasso (grey line, raw data resampled at 1800 s; black line, raw data after removing diurnal and semi-diurnal Earth tides, see also fig. 2 in Amoruso & Crescentini 2010) and expected signal (red dashed line) at the same instrument by the activation of the extensional source of SSE proposed by B16. Strain recorded at BA is not shown, because the expected strain is below the size of transient strain events that can be detected over periods of days to weeks.

influencing both the vertical and horizontal GPS components in reason of respectively elastic response of solid Earth to surface water and anisotropic response of fractured karst aquifers to variations of hydrostatic pore pressure.

Unluckily, the environmental disturbances are not always easily recognizable and may lead to misinterpretation of recorded strain. As an example, many strain transients previously attributed to SSEs triggered by typhoons (e.g. Liu *et al.* 2009) were instead related to environmental noise (e.g. Hsu *et al.* 2015). Thus, error characteristics and common noise source for each geodetic data type have to be carefully evaluated, in order to discriminate between tectonic signals and local effects related to a particular measurement station (e.g. Riel *et al.* 2014).

In this paper, we examine the data recorded in the months preceding the 2009 L'Aquila main shock at both the same local GPS stations used by Borghi *et al.* (2016) and the laser strainmeters, in order to contribute in the understanding of the nature of such recordings potentially related to the claimed aseismic slip episode controlling the timing of earthquake occurrence. To this end, we first reconstruct the signal that the SSE source proposed by Borghi *et al.* (2016, hereinafter B16) would have generated at the two laser strainmeters with the objective of verifying if the generated strain would have been detectable. Then, we explore the local air temperature and precipitation measured during the foreshock sequence close to the GPS station (MTTO) that showed, by far, the largest amount of signal referred to the SSE, in order to show that the GPS displacement transient was most probably related to environmental noise.

2 LOOKING FOR THE SSE SIGNAL WITHIN THE GRAN SASSO STRAINMETERS RECORDINGS

B16 analysed time-series of 29 continuous GPS stations located within about 80 km from the epicentral area of L'Aquila earthquake. The data were divided into two groups composed by data coming from 11 stations located in the near field (see sites location in Fig. 1) and 18 stations in the far field (whose location is not included in Fig. 1). After filtering the data by using the least-squares collocation method (Koch 1977; Moritz 1980), the authors applied the PC analysis to all stations, as well as to the two groups separately (see fig. 2 in B16). The temporal evolution of the first PC for the east displacement of near-field stations results in a nearly exponential signal of few *millimetres* in amplitude starting around the February12 and lasting for about two weeks (see figs 3a and 3b in B16). As established by the authors, the GPS station giving by far the largest contribution to the first PC is MTTO (see fig. 2 in B16). This station, pertaining to the Italian National Geodetic Network managed by the National Institute of Geophysics and Volcanology, is located on top of Mt. Terminillo (location in Fig. 1 and station information at http://ring.gm.ingv.it/?page_id=726&site=MTTO). There is a second station in the near field named OCRA, managed by the Abruzzo region (location in Fig. 1 and station information at http://gnssnet.regione.abruzzo.it/OCRAmono.php?nome=OCRA), contributing to the first PC about half as much as MTTO does, while all the other stations contribute much less. It is worth noting that the nearly exponential signal is essentially visible only in the MTTO east component time-series (see figs S1–S5 in B16). For this reason, we will limit the comparison between displacement and local temperature and precipitation to MTTO.

B16 attribute the signal to an SSE occurred on a complex fault system, consisting of a deep decollement plane composed by four main patches plus two small shallow antithetic faults, combining to generate a total M_w 5.9 event. The proposed fault slip model (reported in Fig. 1) is located to the west of the L'Aquila and Campotosto faults that are the two main fault segments of the 2009 extensional system, as reconstructed by Chiaraluce *et al.* (2011) and Valoroso *et al.* (2013) based on seismicity distribution.

We use the fault model proposed by B16 to compute the strain signal that the SSE source would have generated at the Gran Sasso strainmeters. As in B16, the faults are embedded in a homogeneous elastic half-space and the same Okada (1992) code is used. In this way, strain only depends on the Poisson's ratio of the medium, here assumed to be 0.25. The two orthogonal strainmeters, no longer operating, were based on the classical unequal-arm Michelson interferometer set-up comparing the optical length (i.e. the length expressed in terms of the light wavelength) of a longer measurement arm of 90 m in length, to a shorter and fixed reference arm, which was 20 cm long. Extensions of the measurement arms are given as dimensionless strain $\varepsilon = \Delta l/l$, where l is the baseline length and Δl is positive for an increase in length (1 $n\varepsilon$ is for $\Delta l/l = 10^{-9}$); they are both measured with respect to the baseline length at the starting time of each record. Thus, an arbitrary value can be added to any strain time-series. The instruments were characterized by very high sensitivity, nominally better than 10^{-12} but limited by local noise, very wide frequency band extending from multiyear signals

up to hundreds of *hertz* and large dynamic range, only limited by the capability of maintaining the optical alignment. The interferometers azimuths were N66°E (the one named BC in Fig. 1) and N24°W (BA in Fig. 1; Crescentini *et al.* 1997; Amoruso & Crescentini 2009b). BC and BA were, respectively, oriented almost perpendicular and parallel to the local direction of the Apennines as well as to the geometry of the main fault system activated in 2009 and related SSE.

It is worth noting that comparison between observed and predicted tides shows that tunnel installation and elastic inhomogeneities bias neither strain measurement significantly nor produce significant coupling among the different strain components. However, BC tidal strain is made smaller than predicted by ≈30 per cent by topographic effects (Harrison 1976) because for tides, the scale of topography parallel to BC (the local Apennines width) is much smaller than the scale of the measured stress and strain perturbations (Amoruso & Crescentini 2009b). While BA tidal strain is affected by less than 10 per cent because the scale of topography parallel to BA is not much smaller than the scale of tidal strain. Among many other results (e.g. related to Earth tides, Amoruso *et al.* 2012), these laser interferometers have already produced also clear observations of very small strain transients, for example, in 1997. Tens of slow earthquakes with a cumulative moment magnitude of about M_w 4.8 and characterized by a slow, diffusional slip propagation (Crescentini *et al.* 1999) were recorded during the 1997 Colfiorito seismic sequence occurred about 40 km to the north. Few additional events were observed in succeeding years (see Amoruso *et al.* 2002) and soon after the 2009 L'Aquila earthquake when the characteristics of a slow deforming episode were fully consistent with a slow, diffusional slip propagation toward the shallower portion of the 2009 earthquake causative fault, followed by a few-day long afterslip (Amoruso & Crescentini 2009a).

Since the baselines of the two interferometers were about orthogonal, the size of the signals recorded at BA and BC strongly depends on the relative orientation of the SSE. In case of the SSE source geometry proposed by B16 (and reported in Fig. 1), the amplitude of the strain signal that we computed should have been recorded at BA is about 1 nε, thus below the size of transient strain events that can be detected over periods of days to weeks (fig. 2 in Amoruso & Crescentini 2010). While for BC the expected signal should have been in the order of 90 nε, a value we can demonstrate is certainly detectable because well above the noise level. By looking at the variance $\langle {y_T}^2 \rangle$ of the variation y_T of recorded strain ε_{BC} over a varying time interval T [i.e. $y_T(t) = \varepsilon_{BC}(t+T) - \varepsilon_{BC}(t)$], we can observe the behaviour of the quantity $\langle {y_T}^2 \rangle^{1/2}$ (hereinafter referred to as wander), that can be considered as the resolution limit for strain changes over the different time intervals T (Agnew 1992). Fig. 2(a) shows the wander in strain based on BC data collected between 2008 October and 2009 April (right before the L'Aquila main shock), low-pass filtered and downsampled to 1800 s sampling. We can observe that a 14 d transient signal larger than 22 nε could have been detected against background noise level. A consistent result is obtained by estimating the covariance amplitude for power-law noise given by eq. (11) in Langbein (2004). From Amoruso & Crescentini (2009b), the BC power spectral density based on 45 d strain data collected in 2007 Autumn is approximately given by $2 \times 10^{-5}/f^2$ nε^2 Hz^{-1} in the frequency range 10^{-6}–10^{-2} Hz, and even lower in a subrange around 10^{-4} Hz. Thus, the covariance amplitude is about 0.02 nε $s^{1/2}$, implying a detection threshold of about 22 nε for 14 d.

To better visualize the size of the expected signal, we report in Fig. 2(b), the signal we computed for the SSE source (red dashed line) together with the real data recorded by the interferometer during the same time window, essentially the same data reported in fig. 2 of Amoruso & Crescentini (2010). We have not decreased the SSE strain amplitude by 30 per cent because in this instance the scale of stress and strain perturbations is similar to the scale of topography. From this comparison, it is quite evident that the signal is not present in the temporal evolution of BC strain.

The use of a more realistic Earth model respect to the homogeneous elastic half-space may change the computed transient strain size, but definitely not altering the main conclusion.

3 METEOROLOGICAL DATA

Once we verified the absence of the SSE signal on the two strainmeters, we checked the GPS data and their possible correlation to environmental noise by comparison with the available meteorological data.

As specified by B16, MTTO is responsible for the highest contribution in the first PC, especially for the east component that is the most relevant one in reason of the SSE source geometry. Thus, we looked for meteorological data collected as close as possible to the GPS station. As already mentioned, MTTO is located on top of Mt. Terminillo at about 1736 m of elevation. Luckily, the Monte Terminillo weather station, managed by the *Ufficio Idrografico e Mareografico della Regione Lazio* is located within tens of metres of the GPS site. The data from this station starting from 2007 December are freely available at http://www.idrografico.roma.it/.

Unfortunately, we could not find data regarding the height of the snowline for this time window. But based on the elevation of both the weather and GPS stations (about 1700 m *a.s.l.*), the season (winter), the mean daily temperature (typically below 0 °C; see Fig. 3a) and precipitation (Fig. 3c), there is a high probability that both the GPS and meteorological stations were covered by snow.

Simple yet reasonable physical processes involving temperature and snow close to the GPS station are heating/cooling and water freezing by heat conduction, and snow accumulation and removal because of wind and/or melting during the warmest daylight hours. Thus, we filtered the temperature data of Fig. 3(a) by using a first-order Butterworth low-pass digital filter in order to mimic a simple heat conduction process, namely temperature evolution for a body whose heat exchange is proportional to the difference in temperatures between the body itself and its surroundings, through a constant heat transfer coefficient. The step response of the filter is shown in Fig. 3(b). As regards precipitation, we filter the data of Fig. 3(c) by using a linear digital filter whose impulse response is a decaying exponential (see Fig. 3d). End effects heavily affect both filtered time-series at least during 1 τ from the starting time, where τ is the characteristic time of the filter.

The best fit we found for the characteristic times of the temperature (τ_T) and precipitation (τ_P) filters are 33 and 8 d, respectively. These values have been chosen after chi-square fitting a suitable linear combination of the temperature and precipitation data, filtered for diverse characteristic times, with MTTO east displacement data derived from B16 (see Figs 4a and b) for the two time windows highlighted in Fig. 3(a), referring to the same winter period of the year 2008 and 2009. Misfit dependence on τ_T and τ_P is shown in Fig. 5.

Thus, what we observe for the 2009 time window is that the site hosting the GPS station experienced very cold weather coinciding with the claimed occurrence of the SSE; something quite similar to what occurred during the same winter period in 2008 (Fig. 4b). Furthermore, we find that a linear combination of filtered temperature and precipitation data ($1.36\ T + 0.02\ R$, where T is filtered

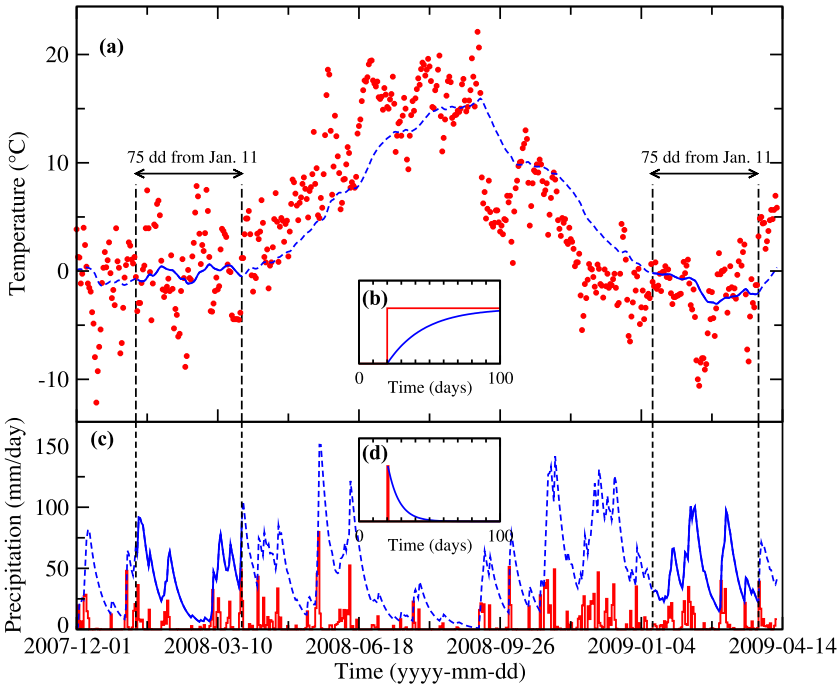

Figure 3. Environmental data recorded by a meteorological station near MTTO. (a) Half-sum of daily minimum and maximum temperatures (red dots) and half-sum of daily minimum and maximum temperatures (blue line) filtered by using a first-order Butterworth low-pass digital filter with characteristic time of 33 d. (b) Step response of the temperature filter. (c) Precipitation as daily measurement (red line) and filtered by using a linear digital filter whose impulse response is a decaying exponential with characteristic time of 8 d (blue line). (d) Impulse response of the precipitation filter. The two time windows inside the double-ended black arrows are the ones we used for comparing GPS east displacement data with environmental noise; lines showing filtered temperature and precipitation time-series are solid inside the two time windows and dashed outside.

temperature in Celsius degrees and R is filtered precipitation in mm d^{-1}) produces an extraordinarily similar signal in MTTO east displacement during both 2008 and 2009 winters and to the east first PC during the winter, 2009, as shown by B16.

Among the other GPS stations, only OCRA, installed on a mediaeval castle, contributes to the first PC for the east component (fig. 2 in B16). According to B16, its SSE east displacement is about −1.6 mm (table 2 in B16); however, the east displacement time-series only evidences a several month long almost linear trend starting from 2008 December (see fig. S5 in B16 and Fig. 4a in this paper), superposed by fluctuations, tenths of millimetres in amplitude. When the linear trend is removed, residual time-series do not show any prominent transient during the SSE occurrence time (Fig. 4a). Supplementary figures in B16 confirm that the hypothesized SSE is not visible on the other GPS stations.

4 DISCUSSION AND CONCLUSIONS

The comparison between the signal that the source of the SSE proposed by Borghi *et al.* (2016) would have generated at the two high-sensitivity laser strainmeters, and the real strain data recorded by these instruments, suggests that such a tectonic episode was highly improbable (see Fig. 2). The presence of elastic heterogeneities introduced by using a more realistic (e.g. 3-D) Earth model may alter the amplitude of computed strain, but are not expected to affect the results of this work. But it seems likely that environmental effects like temperature and precipitation may have largely affected the signal recorded at the GPS station (MTTO) producing so far the only largest visible contribution to the first PC analysis upon which Borghi *et al.* (2016) based their SSE source construction. This hypothesis is corroborated by the strong similarity between the displacement data of MTTO, that following Borghi *et al.* (2016) shows the largest displacement signal and is responsible for the highest contribution in the first PC, and a linear combination of filtered temperature and precipitation data, mimicking simple heat conduction and snow accumulation/removal processes (see Fig. 3). The fact that the same simple linear combination of filtered temperature and precipitation, with the same characteristic times, fits MTTO displacement and the first PC during all the winter time-series shown in Borghi *et al.* (2016) for which temperature and precipitation data are available, namely 2008 and 2009 for MTTO and 2009 for the first PC, is remarkable. Such a correlation between displacement and environmental data is missing during the other seasons, when it neither snows nor freezes. This lack of correlation seems to exclude simple thermal expansion of the bedrock or the pillar monument itself as a local source of deformation. We hypothesize that thermal effects might be caused by ground freezing and consequent water expansion (about 9 per cent) when liquid water is converted into ice. We do not know whether a heavy snowfall occurred during the hypothesized SSE, but the wind was stably blowing from ENE at particularly high speed (up to more than 100 km hr^{-1}, https://www.wunderground.com), possibly accumulating snow in selected places. In addition to this, the analysis of the raw GPS data (RINEX files) performed by using the Teqc code (Estey & Meertens 1999), does not highlight significant variations of multipath-related values (i.e. MP1 and MP2) with respect to yearly average values.

Therefore, our investigation tends to discard the connection between the GPS signals and the occurrence of an SSE, thus implicitly excluding that such aseismic slip may have controlled the timing of the L'Aquila earthquake occurrence.

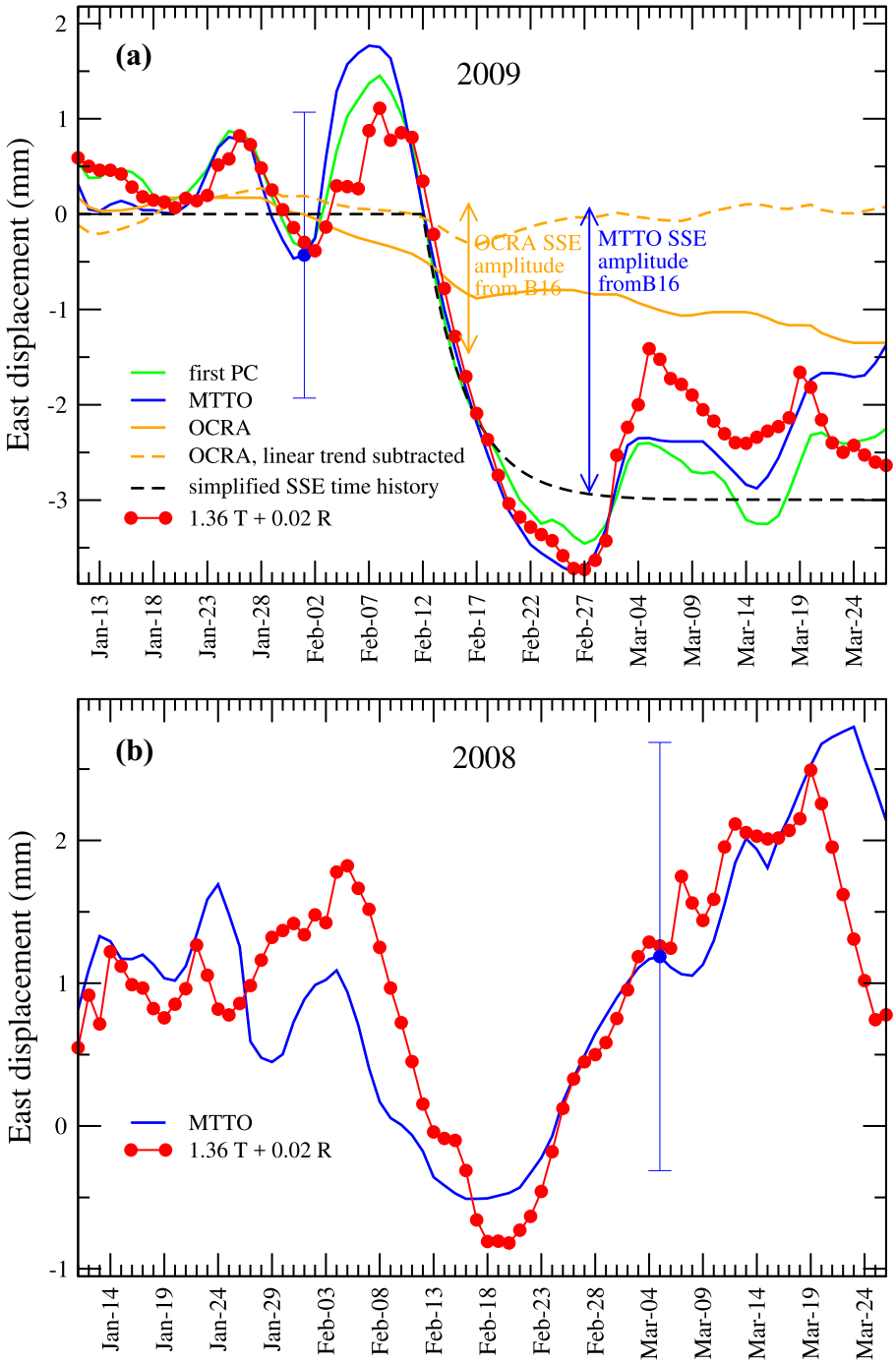

Figure 4. Comparison between east displacement components derived from GPS data and environmental noise, for 75 d starting from the 2009 January 11 in A and 2008 in B. (a) Blue line is MTTO filtered east time-series derived from B16 (fig. S2 in B16); orange solid and dashed lines are OCRA (see fig. S5 in B16) filtered east time-series before and after subtracting the linear trend best fitting the data from 2008 December to 2009 April, respectively. Blue error bar is the GPS data uncertainty from B16. Green line is the first PC. Blue double-ended arrow is the SSE amplitude for MTTO given by table 2 in B16. Orange double-ended arrow is the SSE amplitude for OCRA given by table 2 in B16. Red dots are the best linear combination of filtered temperature and precipitation data, 1.36 $T + 0.02$ R, where T (°C) is filtered half-sum of daily minimum and maximum temperatures (blue line in Fig. 3a) and R (mm d^{-1}) is filtered daily precipitation (blue line in Fig. 3c); units of the regression coefficients are mm (°C)$^{-1}$ and mm (mm d^{-1})$^{-1}$, respectively. Black dashed line in (a) is the simplified SSE time history we used for computing strain at the laser interferometers. All curves are arbitrarily shifted in the y-axis for comparison.

It is worth noting that the time proposed by Borghi *et al.* (2016) for the beginning of the SSE corresponds to the seismicity increase near the L'Aquila main shock hypocentre, during the whole foreshock activity from mid-February to the main shock initiation (Sugan *et al.* 2014). These bursts in seismic activities were also associated with the occurrence of small repeating earthquakes but unfortunately none of these cluster of similar events occurred across the SSE, thus we cannot use them as an indicator of an accelerating or loading process (Valoroso *et al.* 2013). During the foreshock sequence changes in the elastic properties of rocks placed in the fault hangingwall were also observed and were interpreted by some authors as the signature of diffusion processes of highly pressurized fluids

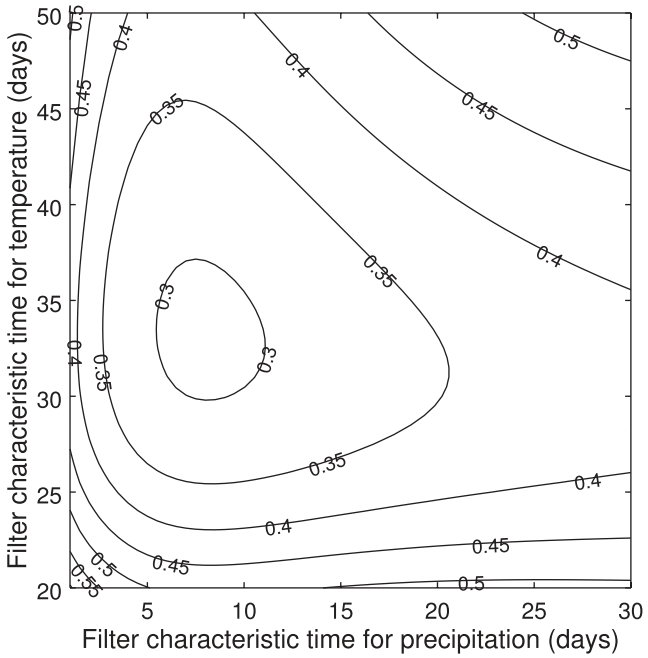

Figure 5. Misfit (mean-squared deviation, mm^2) between a suitable linear combination of the temperature and precipitation data, filtered for diverse characteristic times, and MTTO east displacement data for 75 d starting from the 2008 and 2009 January 11.

(Lucente *et al.* 2010; Terakawa *et al.* 2010). According to Lucente *et al*. (2010), the strongest changes in the V_P/V_S ratio occurred during the last week of the foreshocks sequence, around the March 30, thus after the end of the SSE. While regarding the correspondence in time between the beginning of the SSE and the step in the seismic activity migration toward the main shock hypocentre, we report here that the foreshocks were already migrating from the beginning of January, along the fault plane strike from northwest toward southeast (Chiaraluce *et al.* 2011). At the middle of February, thus during the beginning of the SSE, the migrating seismicity was reaching the main shock (hypocentre) nucleation patch that was characterized by a high V_P and low Poisson ratio (e.g. high V_S body; Di Stefano *et al.* 2011). Thus, the step observed in the seismicity pattern may be also ascribed to the tendency of the seismicity to avoid occurring within such a stiff fault portion, the same reason proposed by Di Stefano *et al*. (2011) for explaining the main shock emergent rupture initiation characterized by a small moment release.

This work shows how environmental noise effects may be subtle and relevant when investigating relatively small strain signals in both space and time and how the availability of data from weather stations and water level sensors colocated with GPS stations may provide critical information which must be taken into consideration while dealing with deformation signals.

ACKNOWLEDGEMENTS

We thank the editor, D.C. Agnew, for helpful comments. The authors also thank J. Langbein and an anonymous reviewer for providing helpful suggestions. We also thank A. Gualandi for improvements of an early version of the manuscript. We acknowledge E. Serpelloni for sharing with us helpful know how about the quality of raw GPS data.

REFERENCES

Agnew, D.C., 1986. Strainmeters and tiltmeters, *Rev. Geophys.,* **24,** 579–624.

Agnew, D.C., 1992. The time-domain behavior of power-law noise, *Geophys. Res. Lett.,* **19,** 333–336.

Agnew, D. & Wyatt, F., 2016. Long-base laser strainmeters: four decades of results, in *Paper Presented at 18th International Symposium on Geodynamics and Earth Tides,* Trieste (Italy), June 5–9.

Amoruso, A. & Crescentini, L., 2009a. The geodetic laser interferometers at Gran Sasso, Italy: recent modifications and correction for local effects, *J. Geodyn.,* **48,** 120–125.

Amoruso, A. & Crescentini, L., 2009b. Slow diffusive fault slip propagation following the 6 April 2009 L'Aquila earthquake, Italy, *Geophys. Res. Lett.,* **36,** L24306, doi:10.1029/2009GL041503.

Amoruso, A. & Crescentini, L., 2010. Limits on earthquake nucleation and other pre-seismic phenomena from continuous strain in the near field of the 2009 L'Aquila earthquake, *Geophys. Res. Lett.,* **37,** L10307, doi:10.1029/2010GL043308.

Amoruso, A., Botta, V. & Crescentini, L., 2012. Free Core Resonance parameters from strain data: sensitivity analysis and results from the Gran Sasso (Italy) extensometers, *Geophys. J. Int.,* **189,** 923–936.

Amoruso, A., Crescentini, L., Martino, S., Petitta, M. & Tallini, M., 2014. Correlation between groundwater flow and deformation in the fractured carbonate Gran Sasso aquifer (INFN underground laboratories, central Italy), *Water Resour. Res.,* **50,** 4858–4876.

Amoruso, A., Crescentini, L., Morelli, A. & Scarpa, R., 2002. Slow rupture of an aseismic fault in a seismogenic region of Central Italy, *Geophys. Res. Lett.,* **29**(24), 2219, doi:10.1029/2002GL016027.

Borghi, A., Aoudia, A., Javed, F. & Barzaghi, R., 2016. Precursory slow-slip loaded the 2009 L'Aquila earthquake sequence, *Geophys. J. Int.,* **205,** 776–784.

Chiaraluce, L., Valoroso, L., Piccinini, D., Di Stefano, R. & De Gori, P., 2011. The anatomy of the 2009 L'Aquila normal fault system (central Italy) imaged by high resolution foreshock and aftershock locations, *J. geophys. Res.,* **116,** B12311, doi:10.1029/2011JB008352.

Crescentini, L., Amoruso, A., Fiocco, G. & Visconti, G., 1997. Installation of a high-sensitivity laser strainmeter in a tunnel in central Italy, *Rev. Sci. Instrum.,* **68,** 3206–3210.

Crescentini, L., Amoruso, A. & Scarpa, R., 1999. Constraints on slow earthquake dynamics from a swarm in central Italy, *Science,* **286,** 2132–2134.

Dal Moro, G. & Zadro, M., 1998. Subsurface deformations induced by rainfall and atmospheric pressure: tilt/strain measurements in the NE-Italy seismic area, *Earth planet. Sci. Lett.,* **164,** 193–203.

Devoti, R., Zuliani, D., Braitenberg, C., Fabris, P. & Grillo, B., 2015. Hydrologically induced slope deformations detected by GPS and clinometric surveys in the Cansiglio Plateau, southern Alps, *Earth planet. Sci. Lett.,* **419,** 134–142.

Díaz, J., Ruíz, M., Crescentini, L., Amoruso, A. & Gallart, J., 2014. Seismic monitoring of an Alpine mountain river, *J. geophys. Res.,* **119,** 3276–3289.

Di Luccio, F., Ventura, G., Di Giovambattista, R., Piscini, A. & Cinti, F.R., 2010. Normal faults and thrusts reactivated by deep fluids: the 6 April 2009 M_w 6.3 L'Aquila earthquake, central Italy, *J. geophys. Res.,* **115,** B06315, doi:10.1029/2009JB007190.

Di Stefano, R., Chiarabba, C., Chiaraluce, L., Cocco, M., De Gori, P., Piccinini, D. & Valoroso, L., 2011. Fault properties heterogeneity affecting the rupture evolution of the 2009 (M_w 6.1) L'Aquila earthquake (Central Italy): insights from seismic tomography. *Geophys. Res. Lett.,* **38,** L10310, doi:10.1029/2011GL047365.

Estey, L.H. & Meertens, C.M., 1999. TEQC: the multi-purpose toolkit for GPS/GLONASS Data, *GPS Solut.,* **3,** 42–49 .

Harrison, J.C., 1976. Cavity and topographic effects in tilt and strain measurements, *J. geophys. Res.,* **81,** 319–328.

Hill, E.M., Davis, J.L., Elósegui, P., Wernicke, B.P., Malikowski, E. & Niemi, N.A., 2009. Characterization of site-specific GPS errors using a short-baseline network of braced monuments at Yucca Mountain, southern Nevada. *J. geophys. Res.,* **114,** B11402, doi:10.1029/2008JB006027.

Hsu, Y.-J. *et al.*, 2006. Frictional afterslip following the 2005 Nias-Simeulue Earthquake, Sumatra, *Science,* **312**(5782), 1921–1926.

Hsu, Y.-J., Chang, Y.-S., Liu, C.-C., Lee, H.-M., Linde, A.T., Sacks, S.I., Kitagawa, G. & Chen, Y.-G., 2015. Revisiting borehole strain, typhoons, and slow earthquakes using quantitative estimates of precipitation-induced strain changes, *J. geophys. Res.,* **120,** 4556–4571.

Ito, Y., Obara, K., Shiomi, K., Sekine, S. & Hirose, H., 2007. Slow earthquakes coincident with episodic tremors and slow slip events, *Science,* **315,** 503–506.

Ito, Y. *et al.*, 2013. Episodic slow slip events in the Japan subduction zone before the 2011 Tohoku-Oki earthquake, *Tectonophysics,* **600,** 14–26.

Ji, K.H. & Herring, T.A., 2012. Correlation between changes in groundwater levels and surface deformation from GPS measurements in the San Gabriel Valley, California, *Geophys. Res. Lett.,* **39,** L01301, doi:10.1029/2011GL050195.

Johnston, M.J.S. (ed.), 1993. The Loma Prieta, California, earthquake of October 17, 1989—preseismic observations, *U.S. Geol. Surv. Prof. Pap. 1550-C*.

Johnston, M.J.S., Borcherdt, R.D., Linde, A.T. & Gladwin, M.T., 2006. Continuous borehole strain and pore pressure in the near field of the 28 September 2004 M 6.0 Parkfield, California, earthquake: implications for nucleation, fault response, earthquake prediction, and tremor, *Bull. seism. Soc. Am.,* **96,** S56–S72.

Koch, K.-R., 1977. Least squares adjustment and collocation, *Bull. Geod.,* **51**(2), 127–135.

Langbein, J., 2004. Noise in two-color electronic distance meter measurements revisited, *J. geophys. Res.,* **109,** B04406, doi:10.1029/2003JB002819.

Linde, A.T., Gladwin, M.T., Johnston, M.J.S., Gwyther, R.L. & Bilham, R.G., 1996. A slow earthquake sequence on the San Andreas fault, *Nature,* **383,** 65–68.

Liu, C., Linde, A.T. & Sacks, I.S., 2009. Slow earthquakes triggered by typhoons, *Nature,* **459**(7248), 833–836.

Lucente, F.P., De Gori, P., Margheriti, L., Piccinini, D., Di Bona, M., Chiarabba, C. & Agostinetti, N.P., 2010. Temporal variation of seismic velocity and anisotropy before the 2009 M_w 6.3 L'Aquila earthquake, Italy, *Geology,* **38,** 1015–1018.

Moritz, H., 1980. *Advanced Physical Geodesy,* Abacus Press, p. 500.

Nadeau, R.M. & Dolenc, D., 2005. Nonvolcanic tremors deep beneath the San Andreas Fault, *Science,* **307,** 389, doi: 10.1126/science.1107142.

Okada, Y., 1992. Internal deformation due to shear and tensile faults in a half-space, *Bull. seism. Soc. Am.,* **82,** 1018–1040.

Prawirodirdjo, L., Ben-Zion, Y. & Bock, Y., 2006. Observation and modeling of thermoelastic strain in Southern California Integrated GPS Network daily position time series, *J. geophys. Res.,* **111,** B02408, doi:10.1029/2005JB003716.

Riel, B., Simons, M., Agram, P. & Zhan, Z., 2014. Detecting transient signals in geodetic time series using sparse estimation techniques, *J. geophys. Res.,* **119,** doi:10.1002/2014JB011077.

Ruiz, S. *et al.*, 2014. Intense foreshocks and a slow slip event preceded the 2014 Iquique M_w 8.1 earthquake, *Science,* **345**(6201), 1165–1169.

Schwartz, S.Y. & Rokosky, J.M., 2007. Slow slip events and seismic tremor at circum-pacific subduction zones, *Rev. Geophys.,* **45,** RG3004, doi:10.1029/2006RG000208.

Scognamiglio, L., Tinti, E., Michelini, A., Dreger, D.S., Cirella, A., Cocco, M., Mazza, S. & Piatanesi, A., 2010. Fast determination of moment tensors and rupture history: what has been learned from the 6 April 2009 L'Aquila earthquake sequence, *Seismol. Res. Lett.,* **81**(6), doi:10.1785/gssrl.81.6.892.

Shearer, P.M., 1994. Global seismic event detection using a matched filter on long period seismograms, *J. geophys. Res.,* **99,** 13 713–13 725.

Silverii, F., D'Agostino, N., Métois, M., Fiorillo, F. & Ventafridda, G., 2016. Transient deformation of karst aquifers due to seasonal and multiyear groundwater variations observed by GPS in southern Apennines (Italy), *J. geophys. Res.,* **121,** 8315–8337.

Sugan, M., Kato, A., Miyake, H., Nakagawa, S. & Vuan, A., 2014. The preparatory phase of the 2009 M_w 6.3 L'Aquila earthquake by improving the detection capability of low-magnitude foreshocks, *Geophys. Res. Lett.,* **41,** doi:10.1002/2014GL061199.

Terakawa, T., Zoporowski, A., Galvan, B. & Miller, S., 2010. High-pressure fluid at hypocentral depths in the L'Aquila region inferred from earthquake focal mechanisms, *Geology,* **38**(11), 995–998.

Valoroso, L., Chiaraluce, L., Di Stefano, R., Piccinini, D., Waldhauser, F. & Schaff, D., 2013. Radiography of a normal fault system by 64,000 high-precision earthquake locations: the 2009 L'Aquila (central Italy) case study, *J. geophys. Res.,* **118,** 1–21.